# Optimum Design for Eddy Current Reduction in Permanent Magnet to Prevent Irreversible Demagnetization

Jae-Woo Jung[1], Sang-Ho Lee[1], Jung-Pyo Hong[1], *Senior Member*, *IEEE*,
Ki-Nam Kim[2], Hyoung-Jun Cho[2], Sang-Hoon Moon[2]
[1]Department of Automotive Engineering, Hanyang University, Seoul, 133-791, Korea
jjw@hanyang.ac.kr, hongjp@hanyang.ac.kr
[2]HEV System Engineering Team, HEV Development Group, Hyundai-Kia Motor, Co. Ltd., Hwaseong, 445-706, Korea

***Abstract*-Irreversible demagnetization which occurs in permanent magnet (PM) due to high temperature is main issue in design of traction motor for hybrid electric vehicle. In order to prevent irreversible demagnetization, eddy current loss in PM should be minimized. This paper deals with the optimum design to reduce eddy current loss in PM. Indirect method is used to instead of direct calculation of eddy current loss which uses 3D transient magnetic field analysis. To estimate eddy current loss indirectly, magneto-static field analysis is employed and the obtained flux density variation in PM is used based on the fact that eddy current loss is proportional to square of flux density and frequency. Response surface methodology coupled with design of experiment is used for optimum design in the objective function of peak-peak value and total harmonic distortion of flux density variation in PM. Motor design process ensuring minimum variation of flux density in PM is presented and a transient analysis is used for verification of optimum design.**

## I. INTRODUCTION

Interior permanent magnet synchronous motor (IPMSM) has both magnetic and reluctance torque and is suitable for flux weakening control, which results it has high power and wide speed range. In order to maximize the power density and size effectiveness, Nd-Fe-B permanent magnet (PM) is generally used in IPMSM [1]. In the design of IPMSM which is applied to traction motor for hybrid electric vehicle (HEV), eddy current loss in PM is important design factor because excessive eddy current in PM seriously affects the motor performance due to irreversible demagnetizing PM [2]. Therefore, eddy current loss in PM should be considered to prevent irreversible demagnetization in the design.

To calculate eddy current loss, transient analysis is required. However, it needs huge computation. Moreover eddy current analysis is 3-dimensional (3D) problem, which implies more time consuming especially for the optimal design. Instead of direct calculation of eddy current loss, the indirect quantity analysis is used in this paper for optimization. The peak-peak value and Total harmonic distortion (THD) of flux density variation in PM is chosen as an objective function for the response surface methodology (RSM) and design of experiment (DOE). Prototype is optimized for eddy current loss minimizing and the design result is verified by 3-D finite element analysis (FEA).

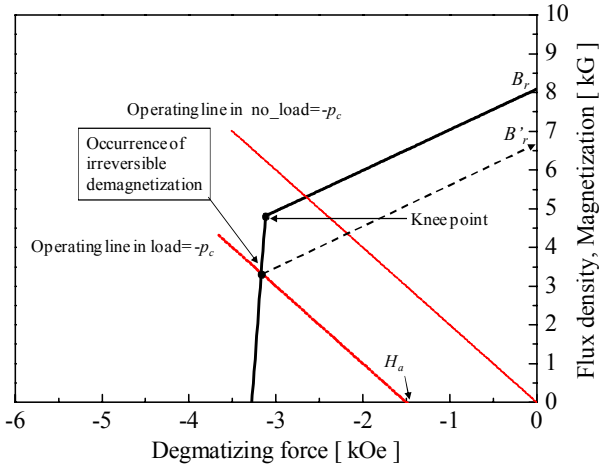


Fig. 1. The variation of flux density in PM

## II. IRREVERSIBLE DEMAGNETIZATION

Irreversible demagnetization of Nd-Fe-B magnet is generally occurs in high temperature. Fig. 1 shows demagnetizing curve of Nd-Fe-B magnet in high temperature over 200℃. Once the load line is located under the knee point, irreversible demagnetization occurs and residual flux density of magnet $B_r$ becomes $B'_r$. The slop of operating line $-P_c$ and reaction magneto-motive force $H_a$ is calculated as follow.

$$\frac{B_m}{H_m} = -P_c \tag{1}$$

$$\frac{N \cdot I_a}{l_m} = H_a \tag{2}$$

where $B_m$ is operating flux density of PM, $H_m$ is operating magnetic intensity of the PM, $N$ is turn per phase, $I_a$ is line current and $l_m$ is PM length of magnetizing direction.

The IPMSM is driven by flux weakening control to ensure high speed operation. In that time, large amount of d-axis current flowed in the stator coil and it generates d-axis magneto-motive force. Then, the load line is located under the knee point as shown in Fig. 1.

The motor which is demagnetized has low back EMF batter than designed value. In this case, line current will be increased to insure same power and efficiency of the motor is decreased due to copper loss rising.

## III. CHARACTERISTICS ANALYSIS

### *A. d-q axis equivalent circuit analysis*

In order to calculate characteristics of IPMSM, d-q equivalent circuit analysis is employed. Equivalent circuit frame including iron loss are presented Fig. 2. The mathematical model of the equivalent circuits is given as follow equations. Iron loss is considered by equivalent resistance $R_c$, and the d- and q-axis voltages and effective torque equations are given by (3), (4) and (5), respectively. Where id and $i_q$ are d- and q-axis component of armature current, $i_{cd}$ and $i_{cq}$ are d-and q-axis component of terminal voltage, $R_a$ is armature winding resistance per phase, $R_c$ is iron loss resistance, $\Psi_a$ is flux linkage of permanent magnet per phase (rms value), $L_d$ and $L_q$ are d-and q-axis armature self inductance, and $P_n$ is pole pair [3].

The line current and current angle of the IPMSM at 6000rpm with 15kW is computed using d-q axis equivalent circuit analysis as shown in Table I.

$$\begin{bmatrix} v_d \\ v_q \end{bmatrix} = R_a \begin{bmatrix} i_{od} \\ i_{oq} \end{bmatrix} + \left(1 + \frac{R_a}{R_c}\right)\begin{bmatrix} v_{od} \\ v_{oq} \end{bmatrix} + p\begin{bmatrix} L_d & 0 \\ 0 & L_q \end{bmatrix}\begin{bmatrix} i_{od} \\ i_{oq} \end{bmatrix} \quad (3)$$

$$\begin{bmatrix} v_{od} \\ v_{oq} \end{bmatrix} = \begin{bmatrix} 0 & -\omega L_q \\ \omega L_d & 0 \end{bmatrix}\begin{bmatrix} i_{od} \\ i_{oq} \end{bmatrix} + \begin{bmatrix} 0 \\ \omega\psi_a \end{bmatrix} \quad (4)$$

$$T = P_n\left\{\psi_a i_{oq} + \left(L_d - L_q\right) i_{od} i_{oq}\right\} \quad (5)$$

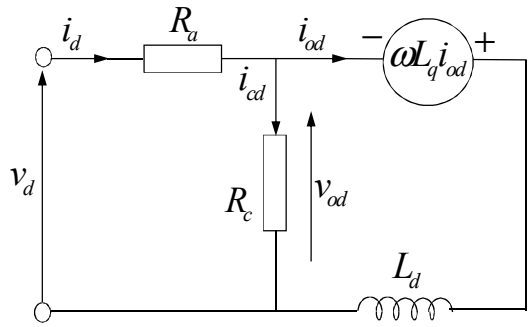


(a) d-axis equivalent circuits

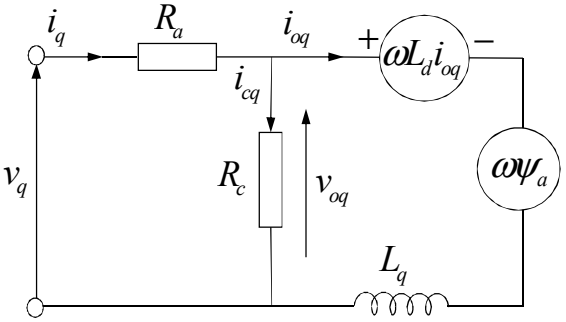


(b) q-axis equivalent circuits

Fig. 2. Equivalent circuit of IPMSM

TABLE I
CALCULATED LINE CURRENT AT 6000RPM

| Speed [rpm] | Line current [$A_{rms}$] | Current angle [° ] | Power [kW] |
|---|---|---|---|
| 6000 | 79 | 72 | 15 |

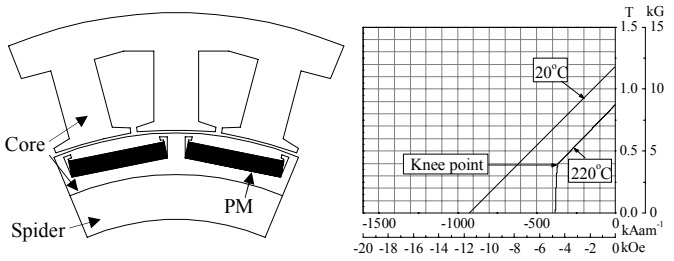


(a) Configuration of prototype (b) Demagnetization curve

Fig. 3. Prototype of optimum design

TABLE II
THE SPECIFICATION OF IPMSM

| Items | Value | Unit | Remark |
|---|---|---|---|
| Input Voltage | 155 | V | DC link |
| Output Power | 15 | kW | Maximum |
| Speed | 6000 | rpm | Maximum |
| Pole / Slot | 16 / 24 | - | Concentrated winding |
| Br | 1.18 | T | 20°C |
| Conductive | 694000 | $\Omega^{-1}$/m | PM |

### *B. Analysis model*

The prototype is IPMSM which is applied in traction motor for mild type HEV. The configuration and specification of prototype is shown in Fig. 3 (a) and Table II, respectably. The PM assembled in the prototype is made from Nd-Fe-B magnet and its demagnetizing curve is shown in Fig. 3 (b). There is no knee point at 20°C but at 220°C its knee point exists at 0.4T. The temperature of the PM is much higher than stator core during high speed operation. Therefore, it can be demagnetized by armature reaction by d-axis current.

## IV. OPTIMUM DESIGN

### *C. Objective Function*

Eddy current is generated by variation of magnetic flux in the conductor and it causes temperature rising. In the case of IPMSM, field weakening control is essential to achieve high speed operation but at the same time the flux density variation occurs in the PM due to the d-axis current as shown in Fig.4 [4]. Supposing that core and PM is insulated electrically, the result of eddy current analysis is shown in Fig. 5. It is computed by 2-D transient analysis of FEA.

Eddy current loss is proportional to square of frequency and amplitude of magnetic flux density. The frequency variation of magnetic flux density in PM is determined by pole and slot combination. Therefore, the frequency cannot be changed unless pole and slot combination is changed. However, peak-peak value and total harmonic distortion (THD) of flux density variation can be minimized by change the geometry of the motor. In this paper, peak-peak value of flux density variation in PM and its THD is selected as objective functions and are given by equation (6), (7). The reason why THD of

flux density variation is selected as an objective function is to reduce the eddy current loss caused by high frequency of flux density variation.

On the other hand, eddy current loss in PM decreases as the number of magnet segment increases [5]. However, more segments imply higher cost.

$$f_{peak-peak} = \frac{\sum_{k=1}^{n} \left(B_{pk-pk}\right)_k}{n} \quad (6)$$

$$f_{THD} = \frac{\sum_{k=1}^{n} (THD)_k}{n} \quad (7)$$

$n$ = 4 (Representive element number)

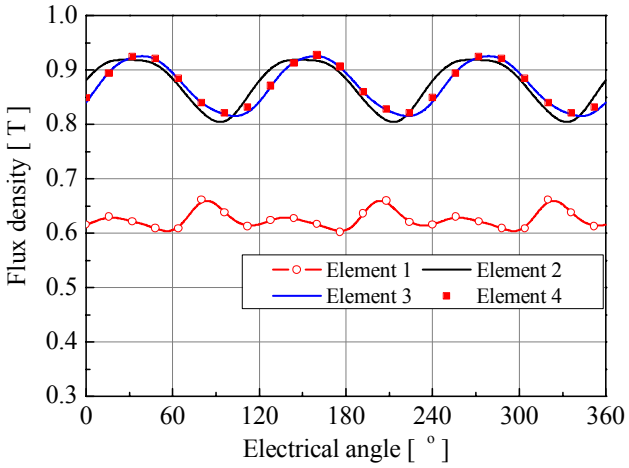


(a) Variation of flux density in PM

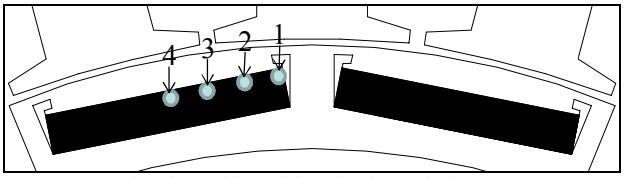


(b) The position of flux density variation

Fig. 4. The variation of flux density in PM

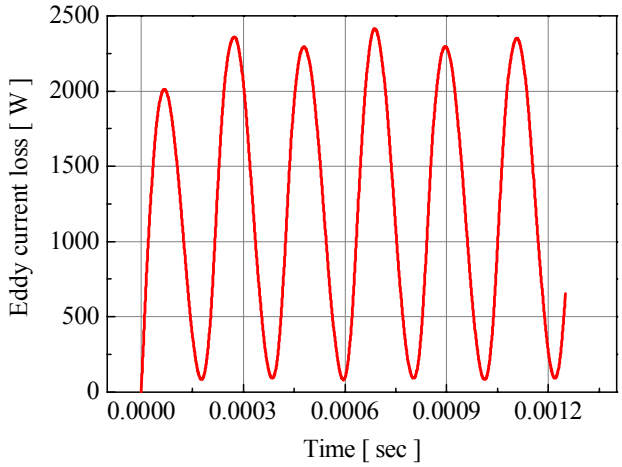


Fig. 5. Eddy current loss in PM (2D transient analysis)

*D. Full Factorial Design*

In order to investigate interaction effects to the objective function, full factorial design (FFD) is employed with 4 design variables which are shown in Fig. 6. The ranges of each design variable are determined and listed in table III.

Generally, the range of design variable for optimization is determined by past experimental data or designer's experience. However, that is apt to make design very restrictive and subjective. Moreover, if the space is established after investigating responses according to the variation of each parameter, a lot of modeling and analysis time is required, and it is difficult to predict the interaction between the parameters. The, $2^4$FFD is applied to obtain more reasonable and objective design range for RSM [6].

Based on the result of $2^4$FFD, design variables and corresponding ranges of RSM are determined. Fig. 7 shows the flux path at the tooth tip according to tooth shape. In order to reduce the flux density variation in the PM, the position of PM is as deep as possible and flux path of the tooth tip should be made as shown in Fig. 7 (a) so that the flux between two teeth can leave from PM.

Fig. 8 shows the interaction effects of all the parameters. The peak-peak value in PM is varied from 0.07T to 0.09T. It is not sensitive and it has few interaction effects with changing variables. However, there are large interaction effects to the THD of magnetic flux density in PM especially produced by chamfer and PM depth. In the RSM, PM depth and Barrier width is fixed as 5.8mm and 1.0mm, respectively to reduce total number of experiments.

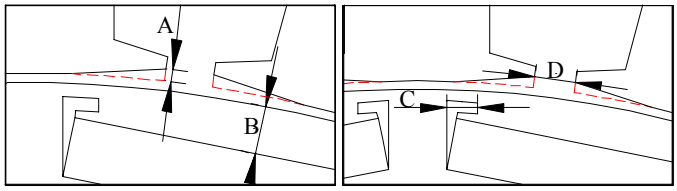


Fig. 6. The design variable of FFD.

TABLE III
THE RANGE OF DESIGN VARIABLE FOR THE FFD

| Symbol | Variable | Range | Unit |
|---|---|---|---|
| A | Chamfer | 0.2-1.0 | mm |
| B | PM depth | 4.0-5.8 | mm |
| C | Barrier width | 1.0-3.0 | mm |
| D | Slot opening | 2.0-4.0 | mm |

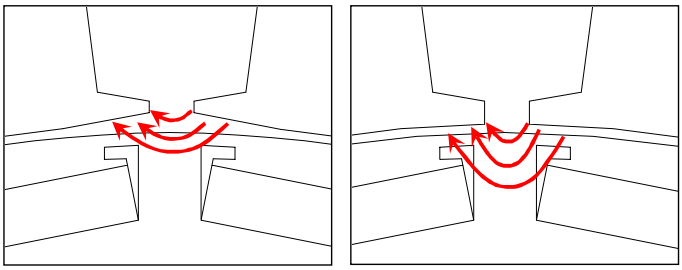

(a) Tooth with chamfer (b) Tooth without chamfer

Fig. 7. Flux path at the tooth tip.

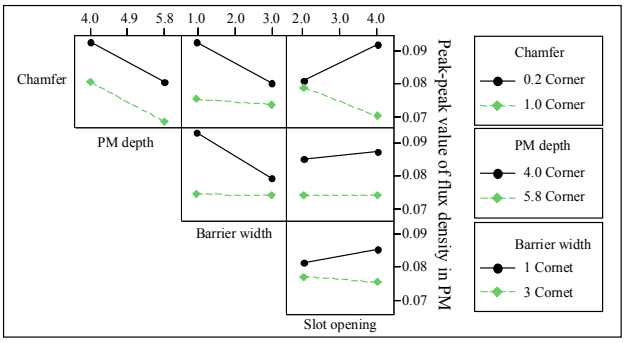


(a) Peak-peak of B in PM

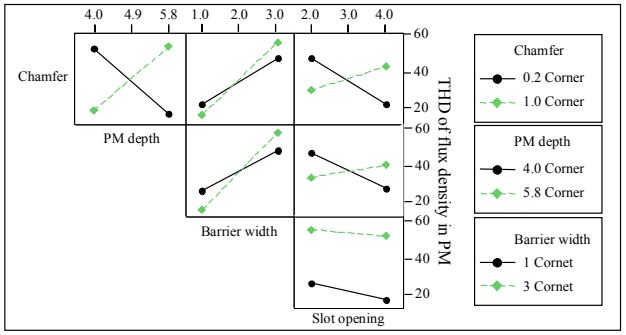


(b) THD of B in PM

Fig. 8. Interaction effect

### *E. Response Surface Methodology*

RSM is applied to make appropriate response models of the peak-peak value and THD of flux density in PM. In this paper, central composite design (CCD) is employed as the experimental design method to estimate the proper model of each response [5].

Based on the result of $2^4$FFD, design variables and range is determined as shown in Table IV. According to CCD, the polynomial models of the responses are given by equation (8) and (9). Fig. 9 shows the response surface for the each objective function. The response surface is useful to know objective function via varying the design variables.

It is possible to raise the current harmonics when the IPMSM is driven with high THD of back EMF, which increases iron loss in magnetic core and eddy current loss in PM. Therefore, THD of back EMF is limited between 3% and 4%, and chosen as a constraint condition in the RSM.

$$\hat{Y}_{peak-peak} = (-92.7 - 188.9B + 120.6C - 15.1BB - 20.1CC + 52.3BC)\times 10^{-3}\ [T] \quad (8)$$

$$\hat{Y}_{THD} = 83.57 + 9.63B - 40.38C + 13.15BB + 5.64CC - 5.64BC\ [\%] \quad (9)$$

TABLE IV
THE RANGE OF DESIGN VARIABLES FOR THE RSM

| Symbol | Variable | Range | Unit |
|---|---|---|---|
| A | Chamfer | 0.2 – 0.6 | mm |
| B | PM depth | 5.8 (Fixed) | mm |
| C | Barrier width | 1.0 (Fixed) | mm |
| D | Slot opening | 3.0 – 4.0 | mm |

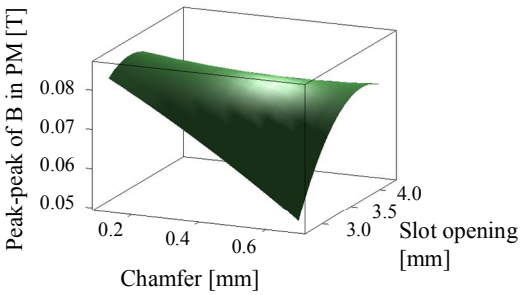


(a) Peak-peak of B in PM

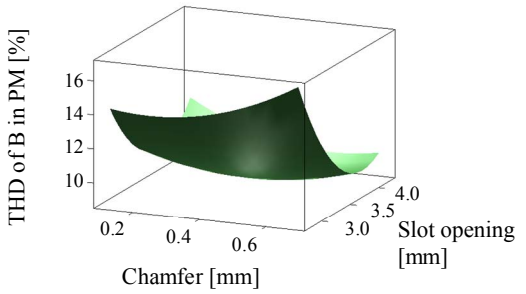


(b) THD of B in PM

Fig. 9. Response surface

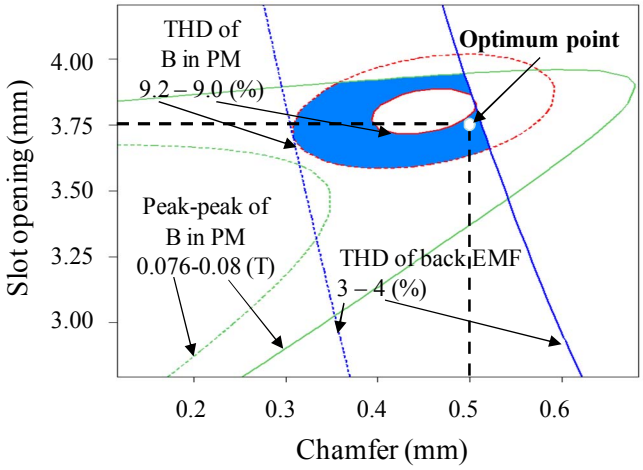


Fig. 10. Optimum point of design variables

Fig. 10 shows the optimum point of design variable with constraint condition. The range satisfying both equation (10) and (11) is displayed in Fig. 10 region. The dot indicates an optimum point minimizing peak-peak value and THD of flux density in PM. Design variables of the prototype and optimum model are compared in Table V. In order to minimize the variation of flux density in PM, PM should be placed in the rotor core deeply.

TABLE V
COMPARISON OF DESIGN VARIABLES

| Variables | Prototype | Optimum model | Unit |
|---|---|---|---|
| Chamfer | 0.2 | 0.5 | mm |
| PM depth | 4.0 | 5.8 | mm |
| Barrier width | 1.0 | 1.0 | mm |
| Slot opening | 2.0 | 3.75 | mm |

$$0.076 \le \hat{Y}_{peak-peak} \le 0.080 \quad (10)$$

$$3 \le \hat{Y}_{THD} \le 4 \quad (11)$$

## V. Result of Optimum Design

### A. Comparison with flux density variation in PM

The optimum model is determined by the optimum design processor. To verify the polynomial model that is found by RSM, the objective function of optimum model is computed using FEA. Table VI shows the comparison of results which are calculated by polynomial models and FEA. There is a good agreement between two results with 5% error. Comparison of flux density variation in each element between the prototype and optimum model is shown in Fig. 11. The peak-peak value and THD of flux density variation is reduced as shown in Table VII. This result means that the eddy current loss in PM is quite reduced.

### B. Comparison of eddy current loss

In order to verify the design method deals in this paper, 3-D FEA is conducted to calculate eddy current loss in PM. Fig. 12 (a) shows the 3-D model of optimum design. The vector and distribution of eddy current is shown in Fig. 12 (b). The result of 3-D FEA about the prototype and optimum model is compared in Fig. 13. Eddy current loss of optimum model is decreased about 50% compared with the prototype. This result shows the design method which is proposed in this paper is expected.

## VI. Result of Optimum Design

The irreversible demagnetization of PM is main issue in the design of IPMSM for the HEV traction motor. In order to prevent irreversible demagnetization in PM, the reduction of eddy current loss in PM is dealt with optimum design process. The eddy current loss of optimum model is decreased about 50% compared with prototype. This result shows that the temperature of PM is also decreased and the possibility of irreversible demagnetization is reduced. In order to calculate exact prediction of irreversible demagnetization, thermal and demagnetizing analysis is required in the further study.

TABLE VI
Comparison with FEA

| Calculating method | Peak-peak of B in PM [T] | THD of B in PM [%] |
|---|---|---|
| Polynomial model | 0.0775 | 9.03 |
| FEA | 0.0752 | 9.42 |

TABLE VII
Comparison between Prototype and Optimum Model

| Model | Peak-peak of B in PM [T] | THD of B in PM [%] |
|---|---|---|
| Prototype | 0.0910 | 46.41 |
| Optimum model | 0.0752 | 9.42 |

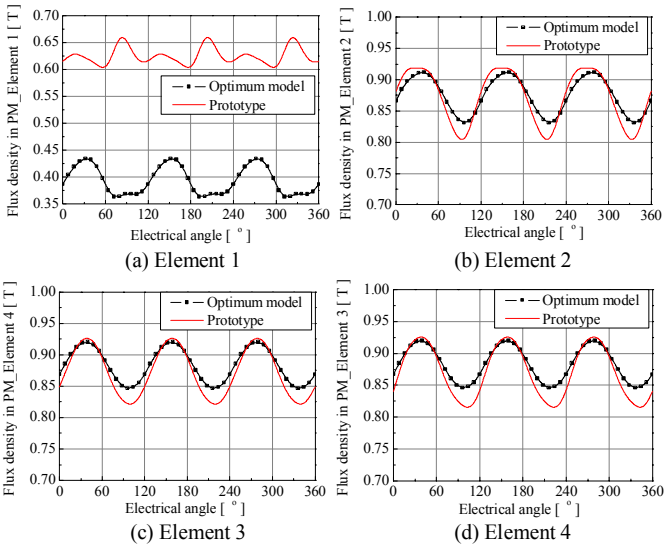


(a) Element 1 (b) Element 2

(c) Element 3 (d) Element 4

Fig. 11. Comparison of the flux density variation in PM

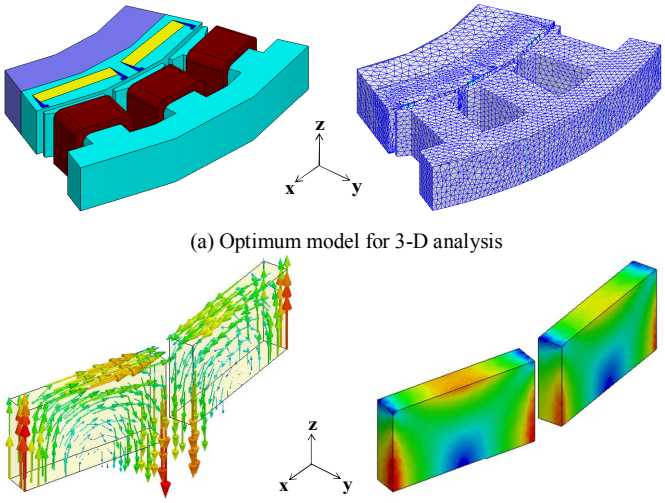


(a) Optimum model for 3-D analysis

(b) Eddy current distribution

Fig. 12. 3-D model for analysis and eddy current distribution

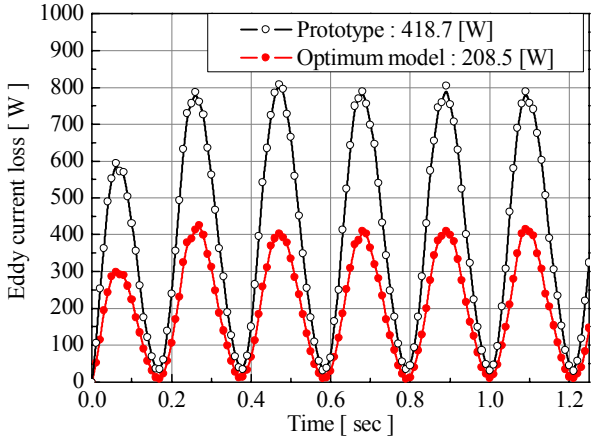


Fig. 13. Comparison of eddy current loss in PM

## REFERENCES


[1] Akira Nishio, Masahiro Hirano, Yoshiki Kato, Takayuki Irie and Tsutomu Baba, "Development of small size light weight and high power IPM motor for electric vehicle," Mitubishi Heavy Industries, Ltd. Technical Review, vol. 40, no. 5, 2003.

[2] Gyu-Hong Kang, Jin Hur, Hyuk Nam, Jung-Pyo Hong and Gyu-Tag Kim, "Analysis of irreversible magnet demagnetization in line-start motors based of the finite element method," *IEEE Trans. Magn.*, vol.39, no. 4, pp.1488-1491, May. 2003.

[3] Ji-Young Lee, Sang-Ho Lee, Geun-Ho Lee, Jung-Pyo Hong and Jin Hur, "Determination of Parameters Considering Magnetic Nonlinearity in an Interior Permanent Magnet Synchronous Motor," *IEEE Trans*., *Magn.*, vol.42, no. 4, pp.1303-1306, April. 2006.

[4] Yoshida. K, Hita. Y and Kesamaru. K, "Eddy current loss analysis in PM of surface mounted PMSM for electric vehicles," *IEEE Trans. Magn.*, vol, 36, no.4, pp. 1941-1944, July. 2000.

[5] Yasuaki Aoyama, Koji Miyata and Ken Ohashi, "Simulations and Experiments of eddy current in Nd-Fe-B magnet," *IEEE Trans. Magn.*, vol. 41, no. 10, pp. 3790-3792, October 2005.

[6] Sung-Il Kim, Jung-Pyo Hong, Young,-Kyoun Kim, Hyuk Nam and Han-Ik Cho, "Optimal design of slotless-type PMLSM considering multiple responses by response surface methodology," *IEEE Trans. Magn.*, vol. 42, no. 4, pp. 1219-1222, April 2006.

# International Conference on Electrical Machines and Systems 2007

October 8 ~ 11, Seoul Olympic Parktel, Seoul, Korea





**Information about how to order the publication :**

KIEE (The Korean Institute of Electrical Engineers)
Room 901, Science & Technology Building, 635-4, Yucksam-Dong, Kangnam-Ku, Seoul
135-703 Korea

Tel: +82-2-553-0151 Fax: + 82-2-566-9957 E-mail: kiee@kiee.or.kr

Organized by

KIEE (The Korean Institute of Electrical Engineers)

Co-organized by

CES (China Electrotechnical Society)

IEEJ (The Institute of Electrical Engineers of Japan)

Technical Co-sponsor

IEEE IEEE Industry Application Society

IEEE Catalog Number : 07EX1815C
ISBN Number : 978-89-86510-07-2
Vendor : Prof. Guee Soo Cha
Tel : +82-41-530-1334 Fax : +82-41-530-1548
E-mail : gsoocha@sch.ac.kr

| | | |
|---|---|---|
| · PMP-27 | **Faults Analysis and Simulation for Interior Permanent Magnet Synchronous Motor Using Simulink@MATLAB**<br>Tao Sun, Suk-Hee Lee, Jung-Pyo Hong | |
| · PMP-28 | **Effect of Rotor Pole Arc Variation on the Performance of Flux Reversal Motor**<br>Pranshu Upadhyay, N. K. Sheth, K. R. Rajagopal | |
| · PMP-29 | **New Proposal of PM-Less Super-High-Speed Blower Motor**<br>Yuta Niwa, Yuji Akiyama, Shinya Manome, Keita Miyazawa | |
| · PMP-30 | **Optimal Design of Electro-Permanent Magnet Lifter Using Improved Niching Genetic Algorithm**<br>Bum-Joo Lee, Sang-Yeop Kwak, Jang-Ho Seo, Sang-Yub Lee, Hyun-Kyo Jung | |
| · PMP-31 | **A Study on Low-Cost Sensorless Drive of Brushless DC Motor for Compressor Using Random PWM**<br>Seung-gun Lee, Dae-kyong Kim, Duck-shick Shin, Byung-taek Kim, Byung-il Kwon, Young-cheol Lim | |
| · PMP-32 | **Starting Mode Analysis of Tubular-type Linear Generator for Free-Piston Engine with Dynamic Characteristics**<br>Young-wook Kim, Jaewon Lim, Ho-Yong Choi, Sun-Ki Hong, Heesoo Lim, Si-Deok Oh, Hyun-Kyo Jung | |
| · PMP-33 | **The Optimization of 60W Linear Motor Using Response Surface Methodology**<br>Do-Kwan Hong, Byung-Chul Woo, Jong-Moo Kim, Jung-Hwan Chang | |
| · PMP-34 | **Development of Multi-layer Interior Permanent Magnet Synchronous Machine for Vehicle**<br>Sang-Yub Lee, Sang-Yeop Kwak, Jang-Ho Seo, Hyun-Kyo Jung | |
| · PMP-35 | **Comparison Evaluation for Permanent Magnet Arrangements of AC Permanent Magnet Contactor**<br>Fang Shuhua, Lin Heyun, Yang Chenfeng, Liu Xiping, Guo Jian | |
| · PMP-36 | **Modeling of End-Effect in Flux-Switching Permanent Magnet Machines**<br>Z. Q. Zhu, J. T. Chen, Y. Pang, D. Howe, S. Iwasaki, R. Deodhar | |
| · PMP-37 | **Optimum Design for Eddy Current Reduction in Permanent Magnet to Prevent Irreversible Demagnetization**<br>Jae-Woo Jung, Sang-Ho Lee, Jung-Pyo Hong, Ki-Nam Kim, Hyoung-Jun Cho, Sang-Hoon Moon | |
| | **Shape Optimization of Rotor Pole in Spoke Type Permanent Magnet Motor for Reducing Partial** | |